Effect of Rayleigh numbers on the evolution of double-diffusive salt fingers

O. P. Singh and J. Srinivasan

Citation: Physics of Fluids (1994-present) **26**, 062104 (2014); doi: 10.1063/1.4882264
View online: http://dx.doi.org/10.1063/1.4882264
View Table of Contents: http://scitation.aip.org/content/aip/journal/pof2/26/6?ver=pdfcov
Published by the AIP Publishing

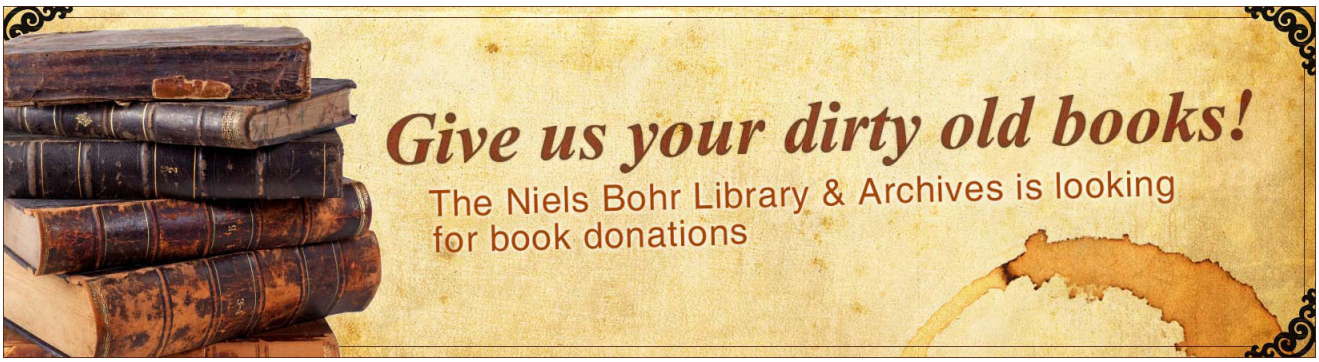

PHYSICS OF FLUIDS **26**, 062104 (2014)

Effect of Rayleigh numbers on the evolution of double-diffusive salt fingers

O. P. Singh[1,a)] and J. Srinivasan[2,b)]
[1]*School of Engineering, Indian Institute of Technology, Mandi 175001, India*
[2]*Centre for Atmospheric and Oceanic Sciences, Indian Institute of Science, Bangalore 560012, India*

(Received 23 July 2013; accepted 20 May 2014; published online 12 June 2014)

This is a transient two-dimensional numerical study of double-diffusive salt fingers in a two-layer heat-salt system for a wide range of initial density stability ratio ($R_{\rho 0}$) and thermal Rayleigh numbers ($Ra_T \sim 10^3 - 10^{11}$). Salt fingers have been studied for several decades now, but several perplexing features of this rich and complex system remain unexplained. The work in question studies this problem and shows the morphological variation in fingers from low to high thermal Rayleigh numbers, which have been missed by the previous investigators. Considerable variations in convective structures and evolution pattern were observed in the range of Ra_T used in the simulation. Evolution of salt fingers was studied by monitoring the finger structures, kinetic energy, vertical profiles, velocity fields, and transient variation of $R_\rho(t)$. The results show that large scale convection that limits the finger length was observed only at high Rayleigh numbers. The transition from nonlinear to linear convection occurs at about $Ra_T \sim 10^8$. Contrary to the popular notion, $R_\rho(t)$ first decrease during diffusion before the onset time and then increase when convection begins at the interface. Decrease in $R_\rho(t)$ is substantial at low Ra_T and it decreases even below unity resulting in overturning of the system. Interestingly, all the finger system passes through the same state before the onset of convection irrespective of Rayleigh number and density stability ratio of the system. © *2014 AIP Publishing LLC*. [http://dx.doi.org/10.1063/1.4882264]

I. INTRODUCTION

When hot and salty water lies over cold and fresh water of a higher density the convective motion gives rise to rising and sinking structures of fluid termed as double diffusive salt fingers (Fig. 1). The potential energy stored in the unstable distribution of one of the component is released due to the difference between the diffusivities of the two components. Depending upon the stratification of the components, convection can either be in diffusive mode or salt finger mode. Salt fingers are formed when the faster diffusing component (denoted as T) contributes to the negative density gradient ($d\rho_T/dz < 0$, stable stratification) and the slower diffusing component (denoted as S) contributes to the positive density gradient ($d\rho_S/dz > 0$, unstable stratification) with overall density stratification remaining gravitationally stable ($d\rho/dz < 0$).

Double diffusive convection has been investigated by many researchers over the years because of its wide application in the various fields of astrophysics, chemistry, geology, metallurgy, meteorology, oceanography, growth of semiconductor crystals.[1–4] The interesting phenomena in these systems are the wide variety of length scales and structures evolve that are controlled by large variations in governing parameters such as Rayleigh numbers. For example, salt fingering mechanism in oceans operates on a length scale of centimeters and time scales in days while the convective structures scale

a)E-mail: om.prakashh.singh@gmail.com. Tel.: +91 1905237992.
b)E-mail: jayes@caos.iisc.ernet.in. Tel.: +91 8022933068.

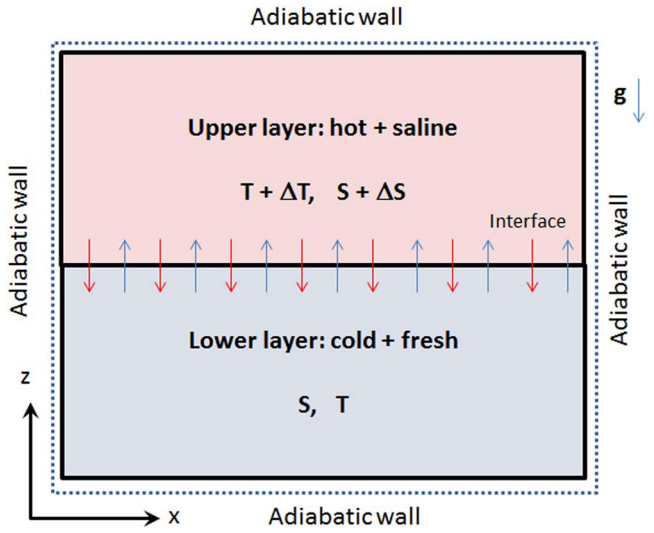

FIG. 1. A schematic diagram of the two-layer computational domain showing initial and boundary conditions.

up to meters over time scales in decades for the columnar-basalt formation in geology.[4] Clearly, the complex mechanism of physics of evolution which has wide applications needs to be understood in a large range of parameters.

Research on salt fingers by previous investigators has mainly concentrated on two important characteristics. First, the variation of flux ratios as a function of density stability ratio and second, finger structures and their evolution. Flux ratio is the ratio between the fluxes of density anomaly due to heat and that due to salt. Recently, Sreenivas *et al.*[5] performed 2D numerical simulations covering a wide range of density stability ratios and Rayleigh numbers. They found that the large scatter in the flux ratio variation reported by various investigators was due to the omission of Rayleigh numbers as primary influencing parameter. Hence, they concluded that at least two of the three governing parameters density stability ratio, salinity or thermal Rayleigh number must be specified to quantify the fluxes transported by fingers.

Second interesting feature of salt fingers is their convective structures and evolution. Salt fingers are generally observed as thin structures sandwiched between the strong horizontal convection that limits the finger amplitudes. Which parameter controls sandwiched structure formation is largely an open question. There is extensive two-layer experiments,[6–10] 2D numerical simulation,[11–17] and 3D numerical simulations[18–20] which investigated this feature of salt fingers evolution. Many theories have been proposed to explain the formation of these sandwich structures or mixed layers separated by salt finger interfaces. Some of these theories are flux ratio instability theory,[21] negative density diffusion,[22] thermohaline intrusion,[23,24] Richardson number constraint,[25] Holyer's theory,[26] collective instability theory,[27] and metastable equilibria.[28] In all these studies, the initial density stability ratio $R_{\rho 0} = \beta_T \Delta T / \beta_S \Delta S$ has been observed to be the most important non-dimensional parameter that controls the finger behavior and specially, the mixed layer formation. Here, β_T and $\beta_S$expansion coefficient for temperature ($^\circ C^{-1}$) and salinity ($\%^{-1}$); ΔT and ΔS are the initial difference in temperature and concentration between the layers (see Fig. 1). There is no clear consensus in the scientific community as to what mechanisms and governing parameters controls the formation of mixed layers and the vertical extent of salt fingers.[29] However, other aspects of this rich and complex finger system such as transient evolution of convective structures from low to high Rayleigh numbers has not been investigated and accounted for in detail.

More than three decades of research on salt fingers has been done in a system where Rayleigh numbers are high[30] of the order of 10^8 or higher.[31] Krishnamurti *et al.*[30] reported laboratory experiments at low Rayleigh numbers and mentioned that the previous investigators rarely observed low Rayleigh numbers[$O(10^3)$] parameters space. The most common observation is thin fingers sandwiched between strong convection that limits the fingers length. The questions of what limits

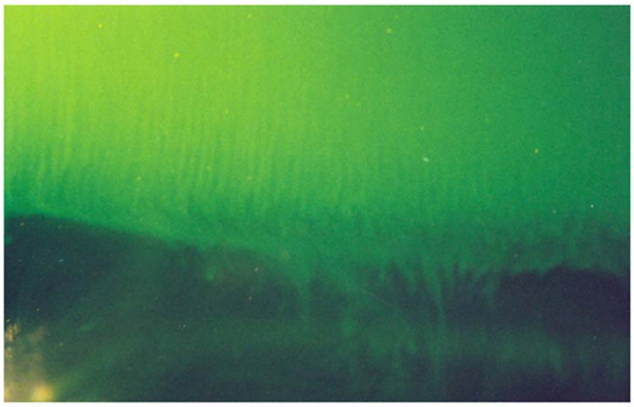

FIG. 2. Snapshot of fingers in a salt-sugar system at high Rayleigh number at time t = 20 min after the start of the experiment. Sugar solution is denoted by lighter-color fluid (top fluid, green online) and salt solution by darker regions (bottom fluid). The system parameters are: $Ra_T = 3.8 \times 10^{11}$, $Ra_S = 1.8 \times 10^{11}$, and $R_{\rho 0} = 2.11$. The ends of the fingers are swept away by horizontal convection. This is a typical characteristic of fingers in high Rayleigh number experiments.

the fingers length is a topic of perennial research. Clearly, salt fingers evolution and their behavior are not yet fully explored in large parameter range of Rayleigh numbers.

Recently, Singh[32] reported convective structures in a two-layer double-diffusive finger system obtained from the laboratory experiments at high thermal Rayleigh number $Ra_T = 3.80 \times 10^{11}$ and moderate $Ra_T = 4.6 \times 10^7$ and are shown in Figs. 2 and 3, respectively. Ra_T is mathematically defined as $Ra_T = g\beta_T \Delta T H^3/\nu k_T$ where ν and k_T are diffusion coefficients for momentum and temperature respectively, g is gravity and H is the domain height. Initially, fingers grow linearly with time and later they become unstable to generate intense convection in the adjoining layers (Fig. 2). It can be noticed from the figure that the ends of the narrow fingers are swept away by the strong shearing convection in the layers that limits the fingers length. At low Rayleigh numbers following features are to be noted (Fig. 3): (a) wide fingers of the order of centimeters evolve, (b) fingers continuously

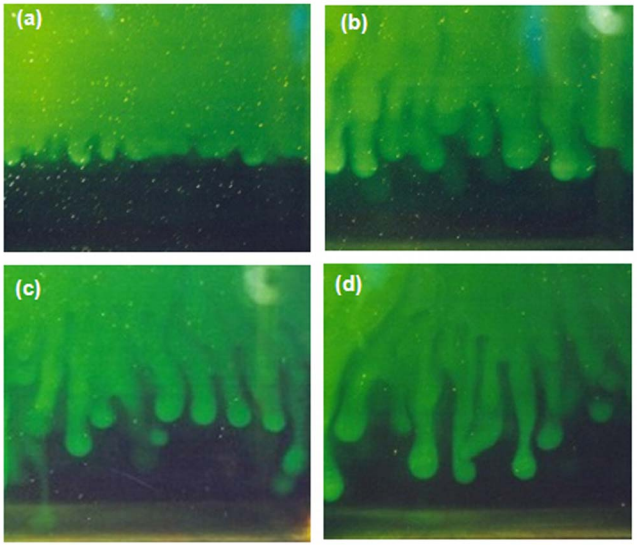

FIG. 3. Time sequence of four photographs showing the evolution of concentration fields in a heat-salt system at lower Ra_T prior to the fingers touching the system boundaries. Fingers widths are of the order of 1 cm. Small shining particles seen in the figures are tiny bubbles formed during layer forming. Parameters of the fluid are $Ra_T = 4.6 \times 10^7$, $Ra_S = 1.0 \times 10^7$, and $R_{\rho 0} = 4.6$. The elapsed time of convection are (a) t = 15 min, (b) t = 22 min, (c) t = 29 min, and (d) t = 36 min. No large scale convection in the layers is seen.

TABLE I. Summary of governing parameters for the series of 25 simulations conducted. Values of Pr, Sc, and τ used are respectively 7, 700, and 100 in all the cases, corresponding to heat-salt system. $R_{\rho 0}$ is the initial density-stability ratio calculated as $R_{\rho 0} = Ra_T/Ra_S$.

Ra_T	3.33×10^9	7×10^8	7×10^7	7×10^6	7×10^5	7×10^4	7×10^3	$R_{\rho 0}\downarrow$
Ra_{S1}		4.667×10^8	4.667×10^7	4.667×10^6	4.667×10^5	4.667×10^4	4.667×10^3	1.5
Ra_{S2}		3.5×10^8	3.5×10^7	3.5×10^6	3.5×10^5	3.5×10^4	3.5×10^3	2
Ra_{S3}	5.55×10^8	1.167×10^8	1.167×10^7	1.167×10^6	1.167×10^5	1.167×10^4	1.167×10^3	6
Ra_{S4}		7×10^7	7×10^6	7×10^5	7×10^4	7×10^3	7×10^2	10

grow and finally reach the top and bottom of the tank, (c) no mixed layer formation is observed, and (d) bulbous finger tips tend to shed off from the parent fingers. In this paper, these behaviors of salt fingers at different Rayleigh numbers has been investigated systematically using 2D numerical simulation. Previous studies have mostly focused on the effect of density stability ratio R_ρ on the evolution of salt fingers.[33,34] Furthermore, many other physical parameters such as system kinetic energy, transient variation of density stability ratio, etc. which are difficult to measure experimentally, have been investigated in this paper in a large range of Ra_T. No attempt has been made in this paper to simulate other complex oceanic processes that undoubtedly exist in the turbulent ocean and other natural and engineering systems.

It is to be noted that 2D numerical simulations differ in magnitude and dynamics with the 3D simulations. For example, 3D fluxes are systematically higher, by a factor of 2–3, than their two-dimensional counterparts.[35] Further, 2D basic state is more unstable than in 3D. Thus, the amplitude of salt fingers is significantly higher in 3D to produce secondary instabilities of the same strength as in two dimensions.[36] Furthermore, convection is expected to take the form of 2D rolls at low Ra_T. Therefore, it is expected that finger evolution process would be different in 3D simulations than in 2D; however, 2D simulations can still provide important insight into the physical processes.

Evolution of salt fingers is also known to be influenced by many non-dimensional parameters (see Sec. II), such as thermal Rayleigh number, Ra_T, salinity Rayleigh numbers, Ra_S, density stability ratio, R_ρ, diffusivity ratio, τ, and Prandtl number Pr. Table I shows the values of these parameters used in this study. The most commonly studied salt finger systems are heat-salt and salt-sugar systems. Heat is the faster diffusing component (about 100 times) and in heat-salt system $\tau \approx 1/100$ and salt is the faster diffusing component (about 3 times faster) in salt-sugar system in which $\tau \approx 1/3$. The stability criterion for finger formation in a two-layer system[37] is

$$1 \ll R_{\rho 0} \ll \tau^{-3/2}. \tag{1}$$

In this paper, effect of Rayleigh numbers on the evolution and structure of salt-fingers in heat-salt system has been presented over a wide range of Ra_T from 10^3 to 10^{10} for initial density stability ratio $R_{\rho 0} = 1.5, 2, 6,$ and 10.

The organization of the paper is as follows. In Sec. II, numerical model for the double-diffusive salt finger convection is presented. Boundary and initial conditions are such that they simulate laboratory two-layer experiments. Results from numerical simulations are presented in Sec. III followed by conclusions in Sec. IV.

II. MATHEMATICAL MODELING

In double-diffusive systems, the fluid density is a function of both components and it is evaluated by[5] $\rho = \rho_0(1 - \beta_T T + \beta_S S)$, where ρ_0 is the reference density of pure water and β_T and β_S are the thermal and salinity expansion coefficients respectively. Variation in density has been considered only in the body force term of the momentum equation and termed as Boussinesq approximation. Thermo-physical properties have been assumed to be constant in the transport equations. The resulting two-dimensional form of the conservation equations of mass (Eq. (2)), momentum

(Eq. (3)), energy (Eq. (4)), and species (Eq. (5)) are, respectively,[5,16,38,39]

$$\Delta \cdot \boldsymbol{U} = 0, \tag{2}$$

$$\frac{\partial \boldsymbol{U}}{\partial t} + (\boldsymbol{U}.\nabla)\,\boldsymbol{U} = -\frac{1}{\rho}\nabla p_d + \nu\nabla^2\boldsymbol{U} - g\,[\beta_S \Delta S - \beta_T \Delta T]\,\boldsymbol{k}, \tag{3}$$

$$\frac{\partial T}{\partial t} + \boldsymbol{U} \cdot \Delta T = k_T \nabla^2 T, \tag{4}$$

$$\frac{\partial S}{\partial t} + \boldsymbol{U} \cdot \Delta S = k_T \nabla^2 S, \tag{5}$$

where $\boldsymbol{U} = (U, W)'$ is the velocity vector, prime denotes matrix transpose; U and W are velocity components in horizontal (x axis) and vertical (z axis) direction; $\boldsymbol{k}$ is the unit vector in the Z-direction, i.e., $\boldsymbol{k} = (0, 1)'$; p_d is the dynamic pressure; ∇, $\nabla.$ And ∇^2 denote gradient, divergence and Laplace operator, respectively, that is,

$$\nabla = \left(\frac{\partial}{\partial X}, \frac{\partial}{\partial Z}\right)', \quad \nabla. = \frac{\partial}{\partial X} + \frac{\partial}{\partial Z}, \quad \nabla^2 = \frac{\partial^2}{\partial X^2} + \frac{\partial^2}{\partial Z^2}.$$

The above set of conservation equations governing the two-dimensional finger-convection system is non-dimensionalised using the following scaling: the depth of the total layer height H is chosen as the characteristic length, velocity (U, W), salinity (S), temperature (T), pressure (p_d) and time (t) are non-dimensionalised as

$$x = \frac{X}{H}, z = \frac{Z}{H}, u = \frac{U}{k_T/H}, w = \frac{W}{k_T/H}, S^* = \frac{S - S_B}{S_T - S_B},$$

$$T^* = \frac{T - T_B}{T_T - T_B}, p = \frac{p_d}{k_T^2 \rho_0 / H^2}, t^* = \frac{t}{H^2/k_T},$$

where (T_T, S_T) and (T_B, S_B) are the temperature and concentration of the top and bottom layers respectively. On introducing the above non-dimensional variables, the governing Eqs. (2)–(5) reduce to the following form:

$$\nabla \cdot \boldsymbol{u} = 0, \tag{6}$$

$$\frac{\partial \boldsymbol{u}}{\partial t^*} + (\boldsymbol{u}.\nabla)\,\boldsymbol{u} = -\nabla p + Pr\nabla^2\boldsymbol{u} - \left[Pr\,Ra_T\left(\frac{S^*}{R_\rho} - T^*\right)\right]\boldsymbol{k}, \tag{7}$$

$$\frac{\partial T^*}{\partial t^*} + \boldsymbol{u}.\Delta T^* = \nabla^2 T^*, \tag{8}$$

$$\frac{\partial S^*}{\partial t^*} + \boldsymbol{u}.\Delta S^* = \frac{Pr}{Sc}\nabla^2 S^*. \tag{9}$$

For simplicity, star in the non-dimensional parameter has been omitted in the following text.

A. Non-dimensional parameters and boundary conditions

An important dimensionless governing derived parameter is the transient density stability ratio $R_\rho(t)$. It is defined as

$$R_\rho(t) = \frac{\beta_T \Delta T(t)}{\beta_S \Delta S(t)} = \frac{Ra_T(t)}{Ra_S(t)}. \tag{10}$$

Salinity Rayleigh number is defined as $Ra_S = g\beta_S \Delta S H^3/\nu k_T$. Note that the definition of Ra_T and Ra_S is such that their ratio produces R_ρ. Other dimensionless parameters are Prandtl number $Pr = \nu/k_T$, Schmidt number $Sc = \nu/k_S$, and diffusivity ratio $\tau = \frac{k_S}{k_T} = \frac{Pr}{Sc}$. The range of the parameters for the series of simulations conducted is shown in Table I. At time $t = 0$, $R_\rho(t) = R_{\rho 0}$ is the initial density stability ratio. For calculating the instantaneous value of $R_\rho(t)$, instantaneous values of ΔT and ΔS are calculated based on the average values of T and S in top and bottom layers. The value of $R_\rho(t)$ defines the strength of stratification of the system. When $R_\rho(t) < 1$, the density gradient is gravitationally unstable (top heavy layer) and the system will overturn. In this paper we will show how the initial $R_{\rho 0} > 1$ can decrease even below unity and its consequence on the finger evolution has been discussed. Note that the parameter τ determines an upper limit for finger formation. It is the ratio of thermal and saline diffusivities and it appears in salinity Eq. (9).

In a two-layer system (Fig. 1) in which hot and saline fluid overlies cold and fresh fluid, the initial profile of the temperature and concentration is a step change in T and S across the interface, at $z = 0.5$. The initial step profiles are chosen to simulate the two-layer laboratory experiments, as most of the previous laboratory experiments reported in the literature have been conducted with a two-layer system. Slip-velocity boundary conditions at sidewalls are applied to simulate infinite layers in horizontal direction; no-slip condition is applied on the top and bottom walls. Since no heat flux was allowed to cross the system boundaries, adiabatic boundary condition was applied on all the four walls. Similar boundary conditions were applied for concentration on all the four walls.

B. Numerical methodology

The computational domain was discritised into small control volumes. The set of non-dimensional governing Eqs. (6)–(9) is integrated over each control volume. The finite volume method and Semi Implicit Method for Pressure-Linked Equations (SIMPLER) algorithm[40] was used for the discretization and solutions of these equations. The equations were split with the use of Alternate Direction Implicit (ADI) method and solutions are obtained by marching in time.

Grid independence study was conducted for different Rayleigh numbers to arrive at optimum grid sizes where convective structures and times scales of evolution do not vary with grids. At highest $Ra_T(= 3.5 \times 10^9)$ the numbers of grids used are 901:401 (x:z) for domain size of aspect ratio 1:1 and it is 301:201 at lowest Rayleigh number ($= 7.0 \times 10^3$) for the same domain size. Detailed validation with experiments and published literature has been reported by Singh[32] and Sreenivas *et al.*[5] Simulations are run even after the fingers have reached the top and bottom boundaries of the computational domain to study the evolution pattern of finger convection.

III. RESULTS AND DISCUSSION

A. Finger structures

In this subsection, salt finger structures are presented for the high and the moderate Rayleigh numbers at the same density stability ratio, $R_{\rho 0} = 6$. The main focus of this section is to show that finger structures can evolve in a significantly different way at different Ra_T similar to that reported in laboratory experiments (Figs. 2 and 3). Finger structures at further lower Rayleigh numbers are presented in the subsequent subsections.

1. Finger structures at high Rayleigh numbers

Fig. 4 shows the time sequence of salinity fields at $Ra_T = 3.33 \times 10^9$ and $R_{\rho 0} = 6$. Attaining higher Ra_T was computationally very expensive and demanding, which requires very fine mesh to resolve the hair-like thin convective structures. Five snapshots are shown here and each snapshot represents five different phases of evolution. It can be seen in Fig. 4(b) that 44 fingers (22 up going; cold and fresh and 22 down coming; hot and saline) are evolved in the domain of aspect ratio 0.33:1 (x:z). The fingers boundaries of these fingers are still not adequately resolved. Animation of fingers from the beginning of the convection to the time when they begin to fade away reveals a rich and

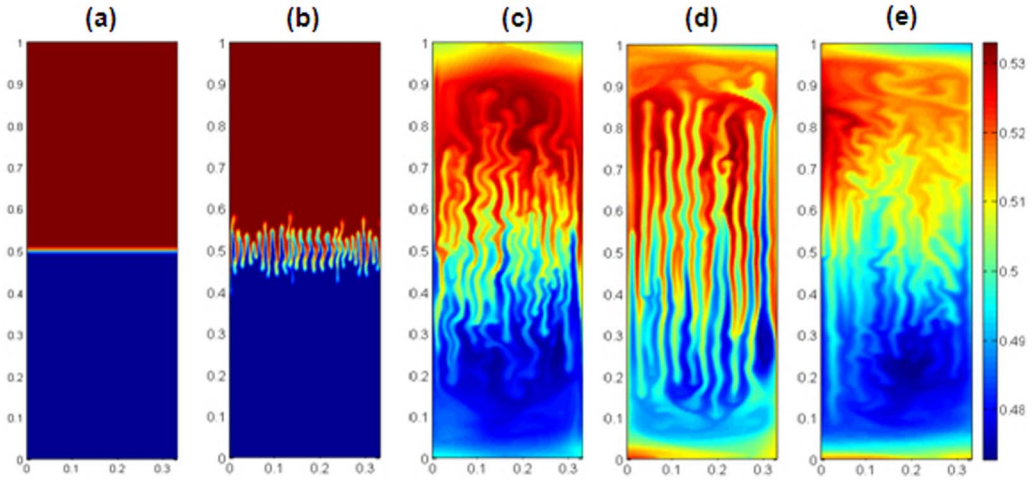

FIG. 4. Time evolution of concentration fields in thermohaline system at high thermal Rayleigh number $Ra_T = 3.33 \times 10^9$and $R_{\rho 0} = 6$, showing five phases of evolution. The five phases and the elapsed time of convection are (a) diffusion phase (I), $t = 3.08 \times 10^{-5}$(b) phase (II): linear evolution of fingers, $t = 3.73 \times 10^{-4}$(c) phase (III): mixed layer formation above and below the finger zone which limits finger growth, $t = 6.60 \times 10^{-3}$(d) phase (IV): strong convection in the mixed layer attenuate and finger starts lengthening again, $t = 1.59 \times 10^{-2}$, and (e) phase (V): finger starts fading away slowly and finger length reduces, $t = 3.69 \times 10^{-2}$.

complex behavior. The system passes through different regimes that can be roughly categorized into five stages of finger evolution:

(i) Diffusive regime where no fingers appears at the interface. Initially sharp interface increases its thickness due to molecular diffusion (time $t = 3.08 \times 10^{-5} \sim 5$ s, Fig. 4(a));
(ii) Instability in the form of thin and slender fingers appears at the interface. Fingers grow linearly with time up to certain height of the domain ($t = 3.73 \times 10^{-4} \sim 60$ s, Fig. 4(b));
(iii) Appearance of large-scale shearing convection in the mixed layers takes place in this regime and the ends of the fingers are swept away by strong horizontal convection in the mixed layers ($t = 6.60 \times 10^{-3} \sim 18$ min, Fig. 4(c));
(iv) Intense convection which was observed in regime III now begins to decrease in its intensity and hence, the fingers' lengths start increasing again ($t = 1.59 \times 10^{-2} \sim 43$ min, Fig. 4(d));
(v) There is now almost uniform concentration distribution in the system, the contrast between the up- and down-going finger decreases and fingers starts fading away ($t = 3.69 \times 10^{-2} \sim 1$ h 40 min, Fig. 4(e)). Lengths of the fingers have reduced in this phase.

The first four phases of evolution are also observed in the laboratory experiments of Singh[32] described in Sec. I at high Rayleigh number. The classification into different phases of evolution is motivated by the experiments of Taylor and Veronis.[33] The quantitative evidence of the above five phases of evolution are shown in Sec. III B using vertical profiles. The last four regimes of the finger evolution described above are well documented.[33] Notice that the first phase persisted for few seconds only. The first phase of evolution, which is the diffusive regime, is not well understood and it is generally considered to be a function of $R_{\rho 0}$. It has been shown later in this paper that it is the first phase that determines the fate of subsequent finger evolution.

2. Finger structures at moderate Rayleigh numbers

Fig. 5 illustrates the evolution of salt fingers at moderate thermal Rayleigh number, $Ra_T = 7 \times 10^6$ and $R_{\rho 0} = 6$. Finger structures at further low Rayleigh numbers have been shown in the later part of the paper. Only 6 fingers are evolved in the domain of aspect ratio 0.33:1 (x:z) compared to 44 fingers at $Ra_T = 3.33 \times 10^9$(Fig. 4). The ratio of finger is 7.33. Recently, Sreenivas *et al.*[5] have shown that fingers width varies as $Ra_T^{-1/3}$ in a two layer system in contrast to a linear system

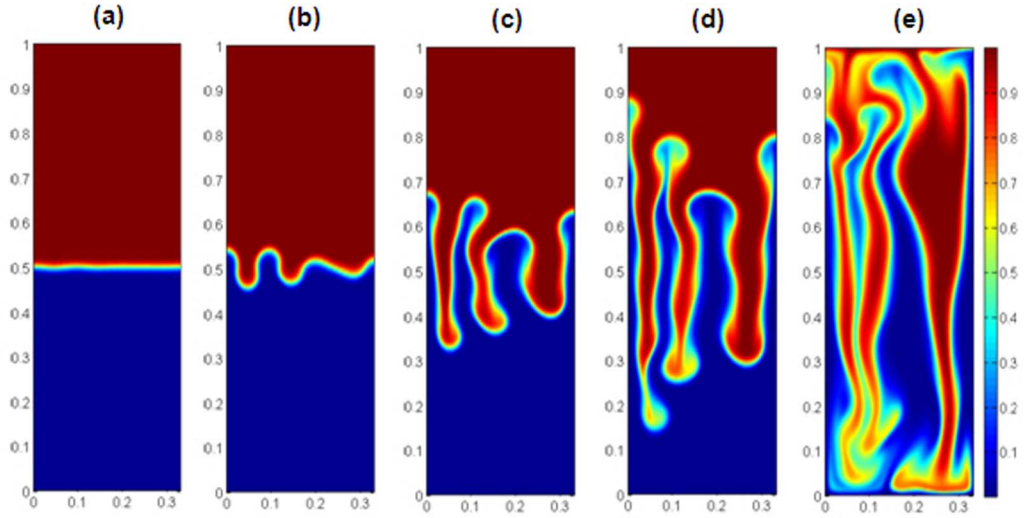

FIG. 5. Time sequence of concentration fields at low thermal Rayleigh number $Ra_T = 7 \times 10^6$and $R_{\rho 0} = 6$. Only two phases of evolution are observed. The first phase is the diffusion phase shown in (a). The second phase is the continuous evolution of fingers. No mixed layer above and below the finger zone is observed. The elapsed time of convection are (a) $t = 3.73 \times 10^{-3}$ (10 min), (b) $t = 5.6 \times 10^{-3}$ (15 min), (c) $t = 8.4 \times 10^{-3}$(22.5 min), (d) $t = 1.12 \times 10^{-2}$ (30 min), and (e) $t = 1.59 \times 10^{-2}$ (42.5 min).

where finger width varies[27] as $Ra_T^{-1/4}$. According to the theory Sreenivas *et al.*, the number of finger expected to evolve at these two Rayleigh numbers is $(3.33 \times 10^9/7 \times 10^6)^{1/3} = 7.8$, in reasonable agreement with the theory. One-third power law variation was also recently reported by Hage and Tilgner.[3]

The evolution pattern is significantly different from that observed at the high Rayleigh number. First, wider fingers evolve at lower Rayleigh number. Second, the increase in finger length is monotonic and they lengthen without interacting dynamically with the neighboring fingers. They finally reach the top and bottom of the computational domain unlike in the case of highestRa_T, where finger growth is hindered by the strong convection in the adjoining regions. Third, the large-scale convection above and below the finger zone observed at high Rayleigh number is not observed at low Rayleigh numbers. Similar observations were made in the laboratory experiments described in Sec. I (see Fig. 3). Contrary to the five phases of finger evolution at high Rayleigh number case (see Fig. 4), only two stages are observed at low Rayleigh number. The first two stages namely the diffusive phase and the linear evolution phase are common for both the high and low Rayleigh numbers.

3. Transition from nonlinear to linear convection

As reported in Subsections III A 1 and III A 2, convective structures differ considerable at high and low Rayleigh numbers. At high Ra_T intense nonlinear convection in the layers was seen that limits the finger length whereas at low Ra_T fingers growth was linear without any shearing convection in the layers. Hence, there must be a narrow range of Rayleigh numbers where this transition occurs. Additional simulations were performed at high Ra_T to figure out the range. Parameters for these simulations are listed in Table II. Figure 6 shows the concentration fields at various Rayleigh numbers. It is to be noticed from the figure that strength of shearing convection in the layers reduces as Rayleigh number reduces. In the range of Rayleigh numbers $3.5 \times 10^9 \geq Ra_T \geq 3.5 \times 10^8$ (Figs. 6(a)–6(e)), fingers deposit sufficient amount concentrations in the layers which might be triggering the shearing convection. However, for $Ra_T \leq 7 \times 10^7$, fingers penetrate into the layer due to the absence of shearing convection. This transition of nonlinear to linear behaviour is observed to lie around the Rayleigh number $Ra_T \sim 10^8$ (in the range of $3.5 \times 10^8 > Ra_T > 7 \times 10^7$).

TABLE II. Additional 4 sets of high Rayleigh numbers at which simulations were carried out in heat-salt system to figure out the ranges of Ra_T where transition from nonlinear to linear convection occurs.

Ra_T	3.5×10^9	2.1×10^9	1.4×10^9	3.5×10^8	$R_{\rho 0}\downarrow$
Ra_S	5.83×10^8	3.5×10^8	2.33×10^8	5.83×10^7	6

B. Vertical profiles and velocity fields

The five phases of evolution described in Fig. 4 at high Rayleigh numbers is shown in terms of vertical profiles of T and S in Fig. 7. Notice that salinity tends to become uniform with time while temperature profile still retains the significant contrast between the layers. For example, in the last phase of evolution at $t = 3.69 \times 10^{-2}$ or 100 min, $\Delta T \sim 0.8$ or 80% temperature contrast

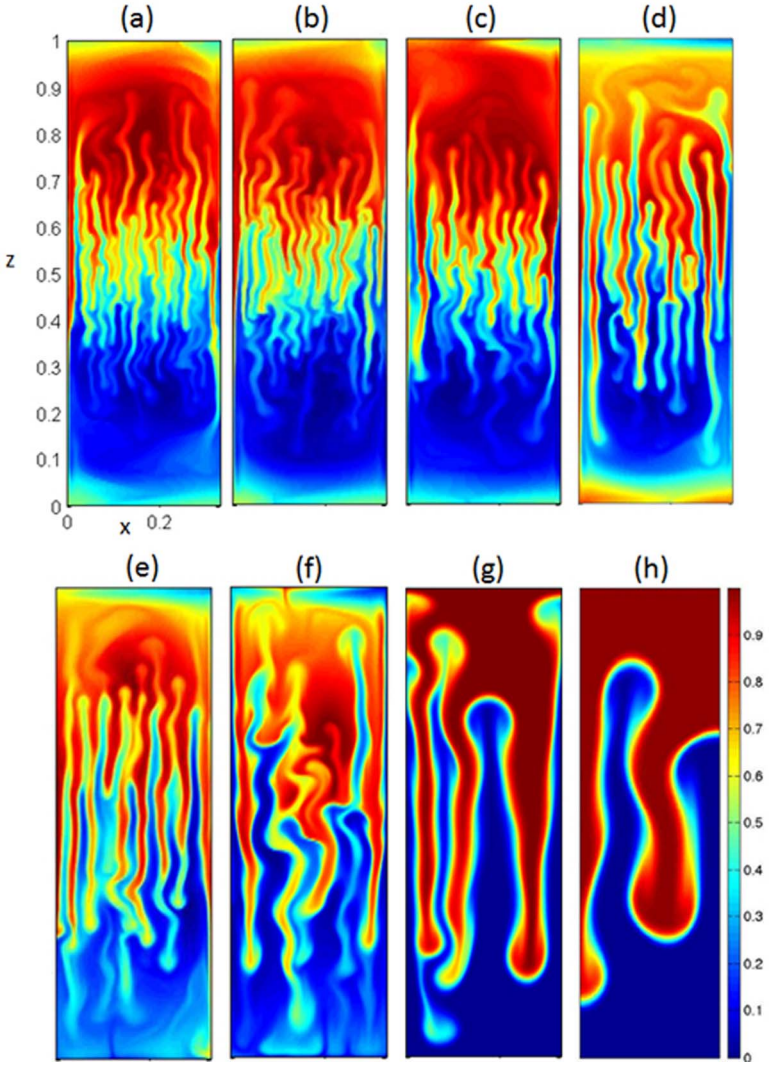

FIG. 6. Concentration fields at $R = 6$ showing convective structures for thermal Rayleigh numbers and time (a) $Ra_T = 3.5 \times 10^9$, $t = 6.50 \times 10^{-3}$, (b) $Ra_T = 2.1 \times 10^9$, $t = 6.50 \times 10^{-3}$, (c) $Ra_T = 1.4 \times 10^9$, $t = 5.60 \times 10^{-3}$, (d) $Ra_T = 7 \times 10^8$, $t = 1.12 \times 10^{-2}$, (e) $Ra_T = 3.5 \times 10^8$, $t = 1.12 \times 10^{-2}$, (f) $Ra_T = 7 \times 10^7$, $t = 1.12 \times 10^{-2}$, (g) $Ra_T = 7 \times 10^6$, $t = 1.31 \times 10^{-2}$, (h) $Ra_T = 7 \times 10^5$, $t = 3.69 \times 10^{-2}$. Notice how the tendency of strong shearing convection formation reduces with Rayleigh numbers.

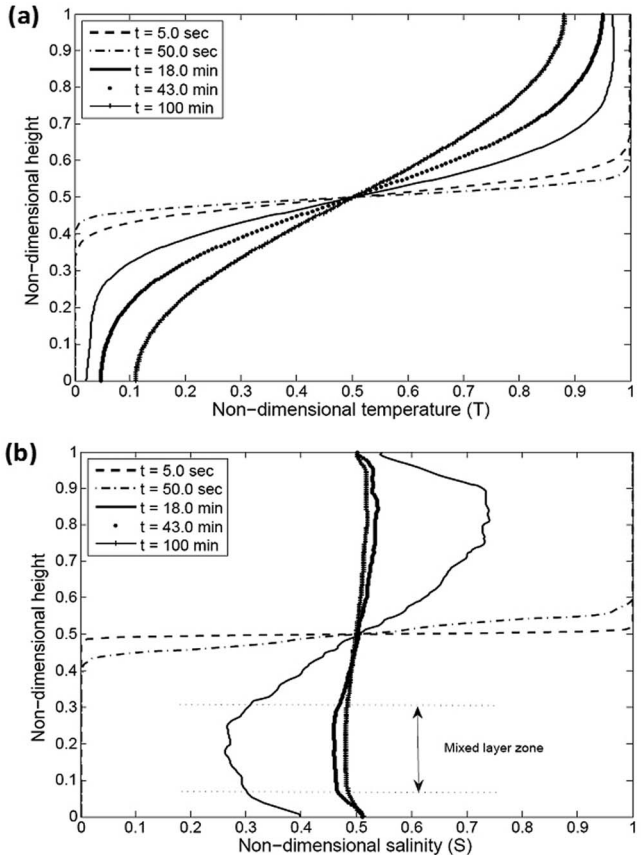

FIG. 7. Vertical profiles of (a) mean temperature $\bar{T}$ at $Ra_T = 3.33 \times 10^9$ for $R_{\rho 0} = 6$ and (b) the corresponding mean salinity $\bar{S}$ profile. With time, the concentration becomes uniform in the layer while temperature still retains the significant temperature contrast between the layers.

between the layers was seen while $\Delta S \sim 0$. With salinity becoming uniform in the layers, the driving force for strong convection in the layers dies down and hence, finger length decreases. When the convection in the layers was intense ($t = 6.60 \times 10^{-3}$or 18 min), formation of mixed layer zone (marked in the figure) is clearly visible. Interestingly, insignificant changes in temperature profile are observed. However, at low Rayleigh numbers (discussed later), the behavior is different (e.g., Fig 10). Figure 8(a) (inset) shows the vertical density profile at high $Ra_T = 3.33 \times 10^9$ at different times and the enlarged view at $0.15 < z < 0.45$ is shown in Fig. 8(b). Time $t = 3.67 \times 10^{-4}$ is the instant when fingers have just evolved at the interface. No large scale convection in the layers is seen at this time. Density inversion (i.e., $d\rho/dz < 0$) can be seen near the interface ($0.35 < z < 0.5$) and rest of the profile is uniform in the layer. However, multiple density inversion points are seen at $t = 1.80 \times 10^{-3}$ when convection is intense in the layer. Note that density of the bottom layer increase with time due to transport of salinity from the top layer.

Instantaneous velocity fields inside the fingers at $Ra_T = 3.33 \times 10^9$ and $Ra_T = 7 \times 10^6$ for $R_{\rho 0} = 6$are shown in Fig. 9. Fig. 9(a) corresponds to the bottom layer of the salinity field at highest Ra_T shown in Fig. 4(d) where shearing convection was observed. Fig. 9(b) corresponds to the bottom layer of the salinity field at moderate Ra_T shown in Fig. 5(d) where no convective mixing was observed. In both the velocity fields, fingers of larger aspect ratio (length to width) with alternatively rising and sinking motions are clearly evident. The main difference between the two velocity fields is in the transition zone from finger regions to the layers. Fingers experience shear in the transition zone as a result of which they tilt in the horizontal direction (Fig. 9(a)). Velocity field at lower Rayleigh number (Fig. 9(b)) shows that tranquil layer away from the finger region is not affected by the fingers. Absence of strong convection in the layer allows fingers to grow and they finally reach

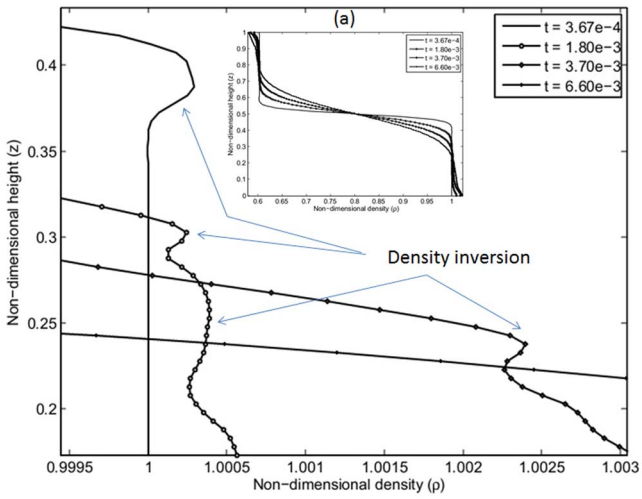

FIG. 8. Expanded view of the vertical density profiles shown in the inset (a) at $Ra_T = 3.33 \times 10^9$at different time. Location of density inversion marked in the figure.

the domain boundaries. The results discussed so far suggest that the finger length limiting process is a high Rayleigh number phenomenon. Laboratory experiments also support this observation.

Vertical profile at further low Ra_T shows altogether different behavior. Fig. 10(a) shows the horizontally averaged mean vertical profiles of T and S at the lowest Rayleigh number ($Ra_T = 7 \times 10^3$and $R_{\rho 0} = 10$) at an instance when the incipient convection has just developed at the interface (see salinity field in Fig. 10(b)). It is noticed that the initial step profile of temperature has become almost uniform without any significant contribution from finger-convection. This is due to the long delay in the onset of convection, which resulted in the significant thermal diffusion in the two layers. Effect of diffusion in the salinity profile can also be seen. However, owing to its lower diffusivity coefficient, modifications in the profile are considerably less compared to the temperature profile as evident from the temperature field (inset Fig. 10(c)). This is a unique characteristic of a thermally diffusion dominated regime. These observations suggest that the top and bottom layers are nearly in thermal equilibrium whereas salinity is still retained in the top layer. Gravitationally, the system is now unstable. The state of a gravitationally unstable finger system can be understood better by monitoring the transient variation of R_ρ at different Rayleigh numbers, which is discussed later.

C. Effect on kinetic energy variation

Velocity in the finger system plays an important role in the transport of convective fluxes of heat and salt across the layers.[5,29] Potential energy stored in the salinity field is released when fingers form. The potential energy is converted into kinetic energy of the system and this energy is finally dissipated by viscosity. Kinetic energy E_k is calculated as

$$E_k = \frac{1}{2}\langle u^2 + w^2 \rangle_D, \tag{11}$$

where $\langle\rangle_D$ denote domain average, u and w are the horizontal and vertical velocities. Fig. 11 shows the evolution of non-dimensional kinetic energy (E_k) as a function of time, i.e., E_k profile for $Ra_T = 7 \times 10^8$ and lowest $Ra_T = 7 \times 10^3$ at a fixed $R_\rho = 2$. Following observations are made:

(i) Magnitude of maximum kinetic energy, $E_{k.max}$, attained by the system decreases with the decrease in Ra_T.
(ii) Fluctuations in the E_k profile, after the system has attained $E_{k,\max}$, decreases with decrease in Ra_T.
(iii) As Ra_T decreases, the E_k profile tends to become symmetric on both sides of the maximum value of E_k.

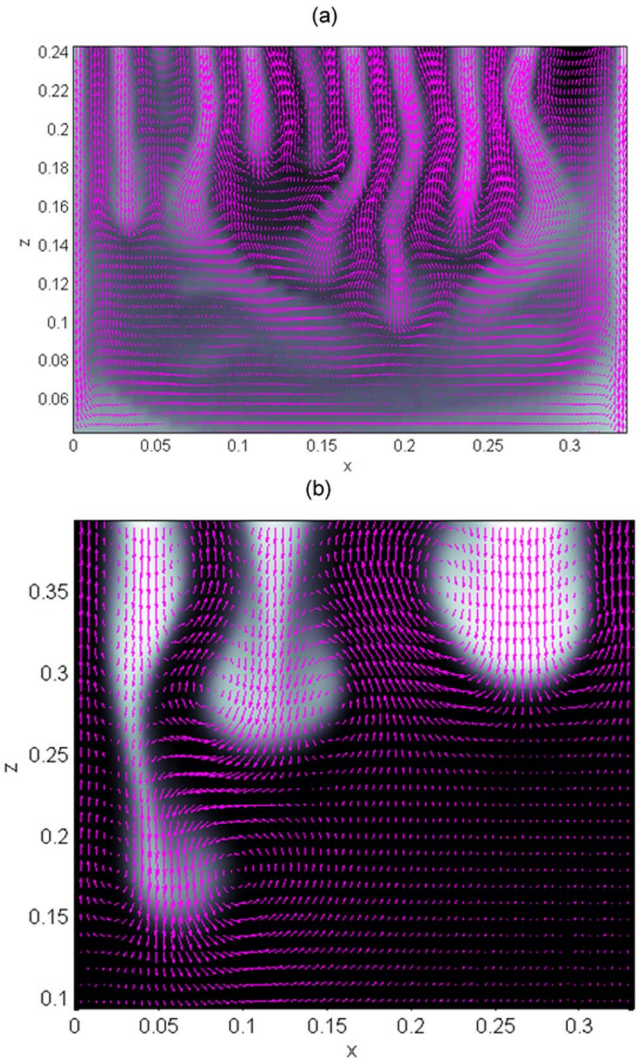

FIG. 9. (a) Velocity field at $0.05 < z < 0.25$ for high $Ra_T = 3.33 \times 10^9$, $R_{\rho 0} = 6$, and time $t = 1.59 \times 10^{-2}$; (b) velocity field at $0.1 < z < 0.4$ for low $Ra_T = 7 \times 10^6$, $R_{\rho 0} = 6$, and $t = 1.12 \times 10^{-2}$.

(iv) Onset time (t_0) of convection at the interface, the time before which $E_k \approx 0$, increases with decrease in Ra_T.

Similar observations were made for other values of $R_{\rho 0}$ (= 1.5, 6, and 10). The first observation suggests that velocity of the finger system can vary considerably even if $R_{\rho 0}$ is held constant. The finger velocity varies with Ra_T and $R_{\rho 0}$ as[5] $w \sim Ra_T^{1/3} R_{\rho 0}$. Fluctuations in the E_k profile at high Ra_T are mainly due to continuous merger of fingers and subsequent generation of new fingers. Further, strong convection in the layers adds to the velocity fluctuation of the system. As Ra_T decreases, these fluctuations cease to exist and the system evolves smoothly. Observation (iii) suggests that at low Rayleigh numbers, the time scale for the dissipation of kinetic energy (from peak value to zero again) is equivalent to the time scale for the production of kinetic energy (from zero to peak value). This is a new observation in finger system.

Another interesting phenomenon [observation (iv)] that can be seen from Fig. 11 is the delay in the onset time of convection (t_0) at the interface as Ra_T decreases. Delay in t_0 was also observed at low Rayleigh number in the laboratory experiments as described in Sec. I. The time t_0 is the time when incipient convection in the form of fingers develops at the initial interface. Over the range

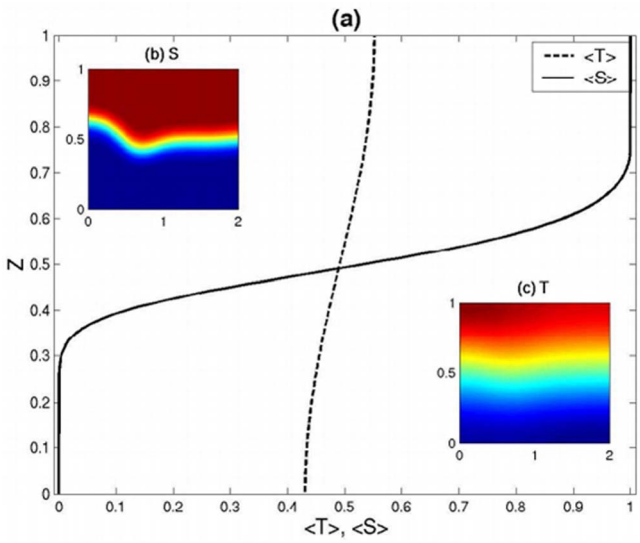

FIG. 10. (a) Horizontally averaged mean T and S profiles as a function of height when the instability at the interface has just appeared for $Ra_T = 7 \times 10^3$ and $R_{\rho 0} = 10$. The elapsed time of convection is 0.235 (10 h 30 min). Shown in the insets are the salinity field S in (b) and temperature field T in (c). Diffusive spread at the interface in the T field can be seen.

of parameters used, effect of Rayleigh numbers on onset of convection was observed to be more pronounced than $R_{\rho 0}$. Laboratory experiments conducted by previous investigators, e.g.,[34,37] were at high Rayleigh numbers where its effect on the system stability is low and hence, the onset of convection of the finger system was studied as a function of $R_{\rho 0}$ alone. Investigations of salt finger systems at low Rayleigh numbers has been missed out by the previous investigators.[30] Effect of delayed onset time on the finger evolution at low Ra_T is discussed in Sec. III D.

D. Effect on density stability ratio variation

1. R_ρ versus time

In a run down two-layer salt finger experiments at high Rayleigh number it has been generally observed that density stability ratio $R_\rho(t)$ monotonically increases with time, e.g., Ref. 6. Increase in $R_\rho(t)$ from the initial value signifies that finger system becomes gravitationally more stable as time progresses. In this section some unique observations are presented about $R_\rho(t)$ variation with time.

Fig. 12 illustrates the variation of $R_\rho(t)$ as a function of time at different Ra_T for initial $R_{\rho 0} = 2$ and 10. Two important observations are made. First, $R_\rho(t)$ decreases for any value of Ra_T before $t < t_0$. After convection in the form of fingers commence at the interface ($t \approx t_0$), R_ρ starts increasing again. Decrease in $R_\rho(t)$ from the initial value of $R_{\rho 0}$ is considerable at lower Ra_T, wherein $R_\rho(t)$ drops even below unity. The consequence of this will be discussed later. Second, $R_\rho(t)$ decreases along a particular diffusion curve for all Ra_T. This means that before the onset of convection the heat-salt finger system passes through the same state irrespective of the Rayleigh number of the system. $R_\rho(t)$ variation was also studied by normalizing $R_\rho(t)/R_{\rho 0}$ for different $R_{\rho 0}$ and Ra_T. All the curves overlap (figure not shown) before $t < t_0$. Hence, it can be generalized that a finger system passes through the same state before the onset of convection irrespective of Rayleigh number and density stability ratio of the system. This is another new observation in salt finger system.

Fig. 13 demonstrates the variation of rate of change of $R_\rho(t)$, i.e., dR_ρ/dt with time for different Ra_T at $R_{\rho 0} = 2$. The slope of dR_ρ/dt for all Ra_T changes from negative to positive signifying that $R_\rho(t)$ decreases first and then increases when convection begins. Furthermore, a sharp change in dR_ρ/dt can be seen indicating a clear onset time of convection in double diffusive finger system. The values of t_0 obtained from dR_ρ/dt plot agrees with those obtained from the kinetic energy plot (see Fig. 11). For example, the value of onset time for $Ra_T = 7 \times 10^8$ is 10^{-4} (Fig. 13) which is same as that was

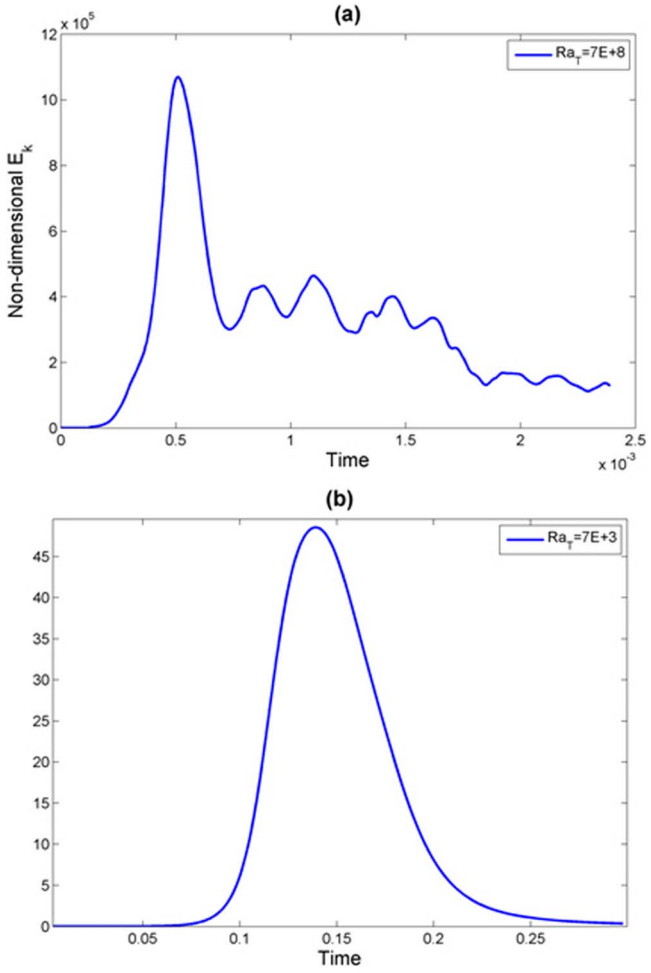

FIG. 11. Evolution of the domain averaged kinetic energy of the system for (a) high $Ra_T = 7 \times 10^8$ and (b) low $Ra_T = 7 \times 10^3$ at a fixed $R_{\rho 0} = 2$. The magnitude of the peak value of kinetic energy decreases with the decrease in Ra_T. The onset timet_0, on the other hand, increases with the decrease in Ra_T.

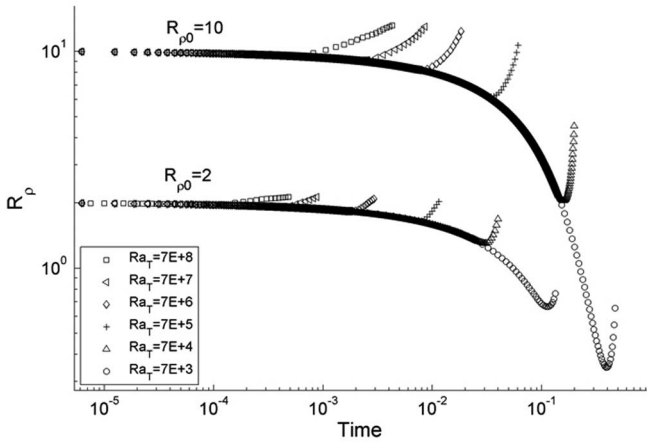

FIG. 12. Variation of density stability ratio $R_\rho(t)$ as function of time at different Rayleigh numbers for initial density stability ratio $R_{\rho 0} = 2$ and $R_{\rho 0} = 10$. Note that $R_\rho(t)$ decreases along the same curve up to the onset time after which it commences to increase.

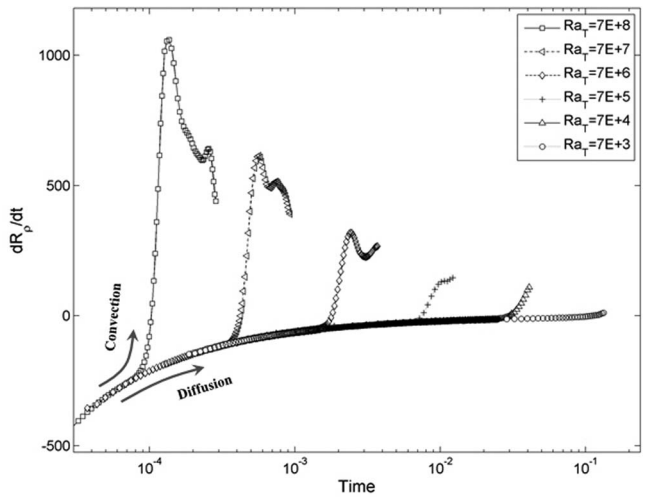

FIG. 13. Transient variation of dR_ρ/dt at various Rayleigh numbers at $R_{\rho 0} = 2$ (see legend). The slope changes from negative to positive for all Ra_T.

obtained from the kinetic energy plot. This is another new and an important observation. Kinetic energy of a system signifies dynamical behavior where as $R_\rho(t)$ signifies gravitational stability of the system and the results demonstrates that they are reciprocally connected. From Fig. 13 it is also noticed that as Ra_T decreases the slope dR_ρ/dt becomes flatter. For $Ra_T = 7 \times 10^3$ the distinction between the diffusion and convection slope is difficult to ascertain. However, the time at which the curve leaves diffusion trend can still be interpreted using both kinetic energy (Fig. 11(b)) and dR_ρ/dt slope.

The diffusion curves collapse onto a single curve and the convection curves (Fig. 13) have similar profiles. In an attempt to figure out suitable time scales that would collapse the convection curves onto a master curve, we tried the time scales discussed by Slim *et al.*[2] Slim *et al.* suggested three time scales (i) the time for diffusion over the whole domain, $t_D = H^2/k_T$, (ii) the time for advection or diffusion over the characteristics distance, $t_{\mathcal{L}} = \emptyset\mathcal{L}/w$ where w is the velocity scale, $w = K\Delta\rho g/\mu$; $K = d^2/12$; d is cell gap width and $\mathcal{L} = k_T/w$ is characteristics length scale over which advection and diffusion balance; $\Phi = 1$, and (iii) the time for advection over the whole domain, $t_H = \emptyset H/w$. The time in Figs. 12 and 13 are scaled with H^2/k_T. Authors also attempted to scale the time by other two scales. For the second case, $t_{\mathcal{L}} = k_T/w^2$. It is to be noted that the velocity scale given by Slim *et al.*[2] and Sreenivas *et al.*[5] (their Eq. (3)) has the same form with $K = d^2/4$; here d is finger width instead of Hele-shaw cell gap width. This velocity scale varies as $w \sim 1.3Ra_T^{1/3}/R_{\rho 0}$ (Eq. (3.3) of Ref. 5) Authors used this velocity scale in $t_{\mathcal{L}}$ and investigated dR_ρ/dt variation (figure not shown). The curves observed to be intersecting at the point of onset time; however, the diffusion and convection curves do not collapse onto a single curve. When scaled with $t_H = H/w$, no collapse was observed in this case as well. The question needs to be put here is: whether there exist a time scale for which convection curve would collapse on to master curve or convection regime in double diffusive salt fingers maintains its unique identity? Further investigations needs to be carried out.

2. Why R_ρ decrease initially

We now provide a physical explanation on why initial $R_{\rho 0}$ decreases initially before the onset of convection and then start increasing when fingers form. Before the onset of instability, only diffusion occurs at the interface. During this period, temperature changes rapidly across the interface while salinity remains virtually unchanged (see Fig. 10). This is due to higher molecular diffusivity of temperature compared to salinity (heat diffuses about 100 times faster). Hence the ratio of $\Delta T/\Delta S$ across the interface decreases and this results in the decrease of R_ρ(Eq. (10)). Longer the delay in the onset time, larger would be the decrease in $R_\rho(t)$ (see Fig. 12). Decrease in $R_\rho(t)$ takes the

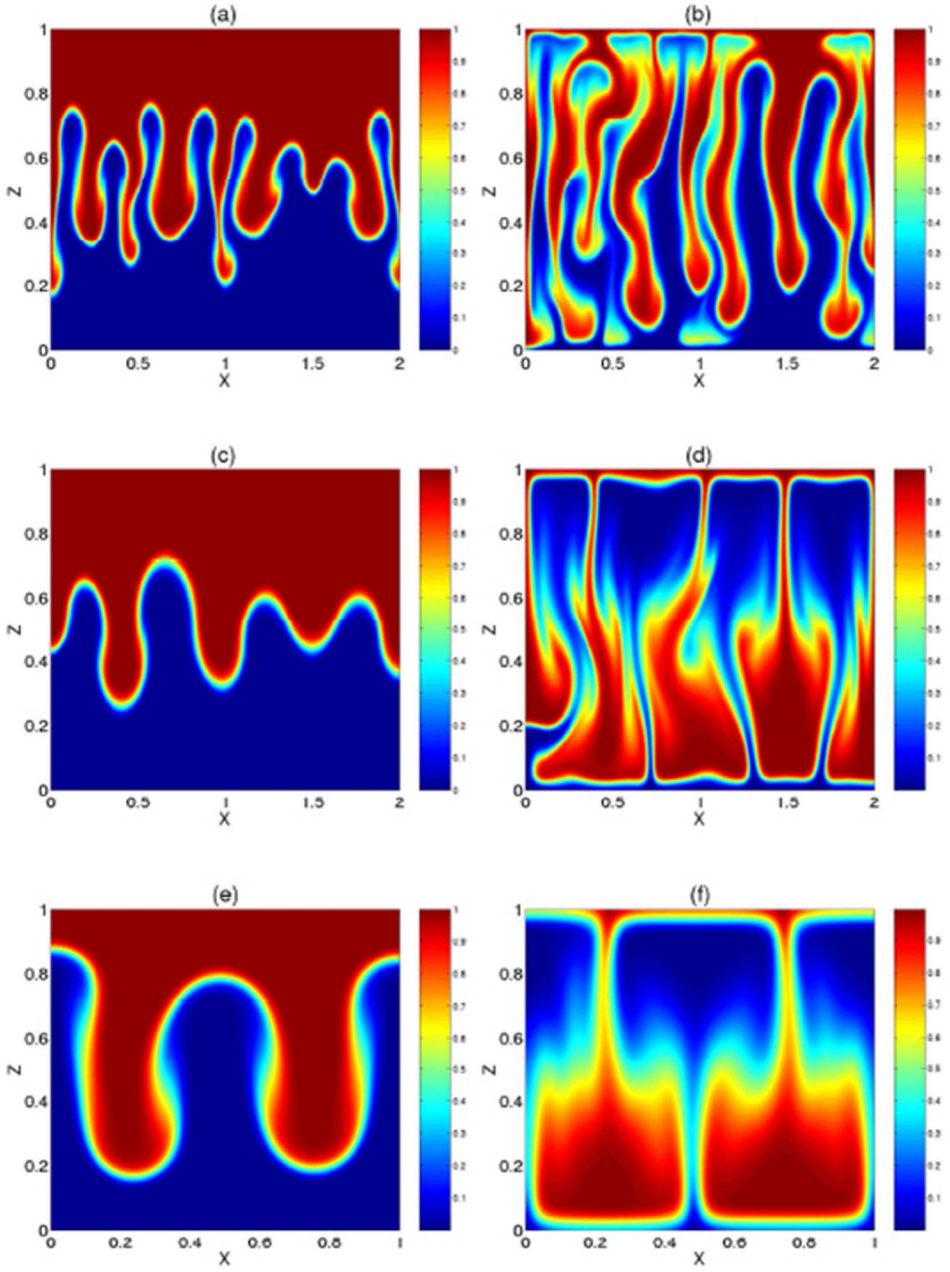

FIG. 14. Salt fingers overturn at low Rayleigh numbers. Figures (all concentration fields) on the left panel show fingers at an instant and their corresponding structures at a later time are shown in the right panel. Thermal Rayleigh number, density stability ratio and elapsed time of convection are respectively for figures (a) and (b) $Ra_T = 7 \times 10^5$, $R_{\rho 0} = 2$, $t = 1.18 \times 10^{-2}$ and 1.8×10^{-2}(c) and (d) $Ra_T = 7 \times 10^4$, $R_{\rho 0} = 1.5$, $t = 2.8 \times 10^{-2}$ and 5.04×10^{-2}, and (e) and (f) $Ra_T = 7 \times 10^4$, $R_{\rho 0} = 10$, $t = 18.67 \times 10^{-2}$ and 26.13×10^{-2}.

system towards a less stable configuration. At low Rayleigh numbers, $R_\rho(t)$ drops below unity after considerable time. $R_\rho(t) < 1$ means that the system is poised for overturning. When convection commences at the interface, the value of ΔSdecreases due to the transport of salinity across the interface by the fingers The ratio $\Delta T/\Delta S$ starts increasing and hence $R_\rho(t)$. It is very difficult to measure the decrease in $R_\rho(t)$ from the initial $R_{\rho 0}$ value in laboratory experiments especially when the diffusivity ratio is low (e.g., salt-sugar system). Further, laboratory experiments are generally conducted at high Rayleigh numbers. At high Rayleigh numbers the onset time is about few seconds

to few minutes depending on the initial $R_{\rho 0}$ value. Typical onset time $t_0 \approx 20$s in the laboratory experiments at high Ra_T (Fig. 2). Furthermore, initial disturbance at the interface makes it more difficult to measure the effect of diffusion in the layers. Properties in the layers are generally measured when the fingers are fully established in the system. Due to these reasons the previous investigators have not observed the decrease in the value of initial $R_{\rho 0}$.

3. Consequence of decrease in R_ρ

As discussed above, fingers at low Rayleigh numbers are more susceptible to overturning as $R_\rho(t)$ drops below unity even before fingers form at the interface. Fig. 14 shows the consequence when fingers are allowed to evolve for a longer period of time at lower Rayleigh numbers. Number of fingers evolved is less compared to high Rayleigh numbers. Salinity fields are shown for three different values of $R_{\rho 0} = 1.5$, 2, and 10. It is evident that fingers have overturned (Figs. 14(d) and 14(f)). By overturning we mean that the initial top layer with hot and saline light fluids is replaced by the bottom layer with cold and fresh heavy fluids and vice versa. It is to be noticed that this overturning process occurs over a large time scale where thermal diffusion dominates in the finger system. Strong convection in the layers is not seen and hence no mixed layer formed. These features are also observed in the laboratory experiments reported by Singh[32] (see Fig. 3).

IV. CONCLUSIONS

Effect of Rayleigh numbers on the evolution of double-diffusive finger convection has been presented using transient two-dimensional numerical simulation in a two-layer heat-salt system for a large range of thermal Rayleigh numbers $Ra_T = 10^3 - 10^{10}$ at density stability ratio $R_{\rho 0} = 1.5, 2, 6,$ and 10. Results show that large scale nonlinear convection that limits the fingers length and forms step-like profile is observed only at high Rayleigh numbers. At low Rayleigh numbers wide fingers evolve and no-large scale convection in the layers was observed for any $R_{\rho 0}$ used in the simulation. The transition from nonlinear to linear convection was observed to occur for Rayleigh number of order of 10^8 (in the range of $3.5 \times 10^8 > Ra_T > 7 \times 10^7$). Kinetic energy of the finger system increases first, reaches a maximum value and then tends to become zero again. The maximum kinetic energy decreases with decrease in Rayleigh numbers. It was observed that as Ra_T decreases, the time scale for the dissipation of kinetic energy (from maximum value to zero again) is equivalent to the time scale for the production of kinetic energy (from zero to peak value). The onset time of convection (t_0) at the interface increases as Rayleigh numbers decrease. The transient variation of $R_\rho(t)$ reveals that $R_\rho(t)$first decreases during the time $t < t_0$ and then increases from the time $t \geq t_0$. Considerable decrease in $R_\rho(t)$ is observed when t_0 is large. $R_\rho(t)$ decrease along the same diffusion curve irrespective of $R_{\rho 0}$ and Ra_T. This feature was also revealed by dR_ρ/dt variation at various Rayleigh numbers. At low Rayleigh numbers $R_\rho(t)$ decreases even below unity resulting in the overturning the finger system. Finally, we remark that this research would be useful to the oceanographers, metallurgist, geologist, study of crystal growth and other research fields where the behavior of double-diffusive systems is govern by the strength of stratification and Rayleigh numbers.

ACKNOWLEDGMENTS

We thank Professor K. R. Sreenivas, Jawaharlal Neheru for Advanced Scientific Research (JNCASR), Jakkur, Bangalore for providing experimental facility and valuable inputs.

[1] R. W. Schmitt, "The characteristics of salt fingers in variety of fluid systems, including stellar interiors, liquid metals, oceans, and magmas," Phys. Fluids **26**(9), 2373–2377 (1983).
[2] A. C. Slim, M. M. Bandi, J. C. Miller, and L. Mahadevan, "Dissolution-driven convection in a Hele-Shaw cell," Phys. Fluids **25**, 024101 (2013).
[3] E. Hage and A. Tilgner, "High Rayleigh nuber convection with double diffusive fingers," Phys. Fluids **22**, 07663 (2011).
[4] O. P. Singh, D. Ranjan, J. Srinivasan, and K. R. Sreenivas, "A study of basalt fingers using experiments and numerical simulations in double-diffusive systems," J. Geogr. Geol. **3**(1), 42–50 (2011).

[5] K. R. Sreenivas, O. P. Singh, and J. Srinivasan, "On the relationship between finger-width, velocity and fluxes in thermohaline convection," Phys. Fluids **21**(2), 026601–026615 (2009).
[6] J. S. Turner, "Salt fingers across a density interface," Deep-Sea Res. **14**, 599–611 (1967).
[7] P. F. Linden, "On the structure of salt fingers," Deep-Sea Res. **20**, 325–340 (1973).
[8] R. W. Schmitt, "Flux measurements on salt fingers at an interface," J. Mar. Res. **37**, 419–436 (1979).
[9] T. J. McDougall and J. R. Taylor, "Flux measurements across a finger interface at low values of the stability ratio," J. Mar. Res. **42**, 1–14 (1984).
[10] J. Taylor and P. Bucens, "Laboratory experiments on the structure of salt fingers," Deep-Sea Res. **36**, 1675–1704 (1989).
[11] D. W. A. Whitfield, G. Holloway, and J. Y. Holyer, "Spectral transform simulations of finite amplitude double-diffusive instabilities in two dimensions," J. Mar. Res. **47**, 241–265 (1989).
[12] S. A. Piacsek and J. Toomre, "Nonlinear evolution and structure of salt fingers," in *Marine Turbulence*, Elsevier Oceanography Series Vol. **28**, edited by J. C. J. Nihoul (Elsevier, 1980), pp. 193–219.
[13] C. Y. Shen, "The evolution of the double-diffusive instability: Salt fingers," Phys. Fluids **1**, 829–844 (1989).
[14] C. Y. Shen, "Heat-salt finger fluxes across a density interface," Phys. Fluids **5**, 2633–2643 (1993).
[15] C. Y. Shen and G. Veronis, "Scale transition of double-diffusive finger cells," Phys. Fluids **3**, 58–68 (1991).
[16] C. Y. Shen and G. Veronis, "Numerical simulations of two-dimensional salt-fingers," J. Geophys. Res. **102**, 23131–23143, doi:10.1029/97JC01580 (1997).
[17] T. M. Ozgokmen and O. E. Esenkov, "Asymmetric salt fingers induced by a nonlinear equation of state," Phys. Fluids **10**, 1882–1890 (1998).
[18] T. Radko and M. E. Stern, "Finite-amplitude salt fingers in a vertically bounded layer," J. Fluid Mech. **425**, 133–160 (2000).
[19] A. Traxler, S. Stellmach, P. Garaud, T. Radko, and N. Brummell, "Dynamics of fingering convection. Part 1 Small-scale fluxes and large-scale instabilities," J. Fluid Mech. **677**, 530–553 (2011).
[20] S. Kimura and W. Smyth, "Direct numerical simulation of salt sheets and turbulence in a double-diffusive shear layer," Geophys. Res. Lett. **34**, L21610, doi:10.1029/2007GL031935 (2007).
[21] T. Radko, "A mechanism for layer formation in a double-diffusive fluid," J. Fluid Mech. **497**, 365–380 (2003).
[22] R. W. Schmitt, "Double diffusion in oceanography," Annu. Rev. Fluid Mech. **26**, 255–285 (1994).
[23] W. J. Merryfield, "Origin of thermohaline staircases," J. Phys. Oceanogr. **30**(5), 1046–1068 (2000).
[24] B. Ruddick and O. Kerr, "Oceanic thermohaline intrusions: Theory," Prog. Oceanogr. **56**, 483–497 (2003).
[25] E. Kunze, "Limits on growing, finite-length salt fingers: A Richardson number constraint," J. Mar. Res. **45**, 533–556 (1987).
[26] J. Y. Holyer, "The stability of long, steady two-dimensional salt fingers," J. Fluid Mech. **147**, 169–185 (1984).
[27] M. E. Stern, "Collective instability of salt fingers," J. Fluid Mech. **35**, 209–218 (1969).
[28] M. E. Stern and J. S. Turner, "Salt fingers and convecting layers," Deep-Sea Res. **16**, 497–511 (1969).
[29] E. Kunze, "A review of oceanic salt-fingering theory," Prog. Inoceangr. **56**, 399–417 (2003).
[30] R. Krishnamurti, Y. H. Jo, and A. Stocchino, "Salt fingers at low Rayleigh numbers," J. Fluid Mech. **452**, 25–37 (2002).
[31] D. E. Kelley, "Fluxes through diffusive staircases: A new formulation," J. Geophys. Res. **95**, 3365–3371, doi:10.1029/JC095iC03p03365 (1990).
[32] O. P. Singh, "Dynamics of double diffusive finger convection: Structures and convective fluxes," Doctoral thesis (Indian Institute of Science, Bangalore, India, 2006).
[33] J. Taylor and G. Veronis, "Experiments on double-diffusive sugar-salt fingers at high stability ratio," J. Fluid Mech. **321**, 315–333 (1996).
[34] C. A. Cooper, R. J. Glass, and S. W. Tyler, "Effect of buoyancy ratio on the development of double- diffusive finger convection in a Hele-Shaw Cell," Water Resour. Res. **37**(9), 2323–2332, doi:10.1029/2001WR000343 (2001).
[35] M. E. Stern, T. Radko, and J. Simeonov, "Three-dimensional salt fingers in an unbounded thermocline with application to the central ocean," J. Mar. Res. **59**, 355–390 (2001).
[36] T. Radko and D. Paul Smith, "Equilibrium transport in double-diffusive convection," J. Fluid Mech. **692**, 5–27 (2012).
[37] H. E. Huppert and P. C. Manins, "Limiting conditions for salt fingering at an interface," Deep-Sea Res. **4**, 553–560 (1973).
[38] T. Radko and M. E. Stern, "Salt fingers in three dimensions," J. Mar. Res. **57**, 471–502 (1999).
[39] J. Yoshida and H. Nagashima, "Numerical experiments on salt-finger convection," Prog. Oceanogr. **56**, 435– 459 (2003).
[40] S. V. Patankar, *Numerical Heat Transfer and Fluid Flow* (Hemisphere Publishing company, New York, 1980).